Transport in Porous Media **49:** 209–240, 2002.

Numerical Simulation of Single-Phase and Multiphase Non-Darcy Flow in Porous and Fractured Reservoirs

YU-SHU WU
Earth Sciences Division, Lawrence Berkeley National Laboratory, CA 94720, Berkeley, U.S.A.

(Received: 5 February 2001; in final form: 28 May 2001)

Abstract. A numerical method as well as a theoretical study of non-Darcy fluid flow through porous and fractured reservoirs is described. The non-Darcy behavior is handled in a three-dimensional, multiphase flow reservoir simulator, while the model formulation incorporates the *Forchheimer* equation for describing single-phase or multiphase non-Darcy flow and displacement. The non-Darcy flow through a fractured reservoir is handled using a general dual-continuum approach. The numerical scheme has been verified by comparing its results against those of analytical methods. Numerical solutions are used to obtain some insight into the physics of non-Darcy flow and displacement in reservoirs. In addition, several type curves are provided for well-test analyses of non-Darcy flow to demonstrate a methodology for modeling this type of flow in porous and fractured rocks, including flow in petroleum and geothermal reservoirs.

Key words: non-Darcy flow, numerical reservoir simulation, well tests, multiphase flow, porous and fractured reservoirs.

Nomenclature

a	dimension of 1-D matrix blocks or x-directional dimension for 2-D or 3-D matrix blocks (m).
b	y-directional dimension for 2-D or 3-D matrix blocks (m).
c	z-directional dimension for 3-D matrix blocks (m).
C_{f}	fluid compressibility (Pa^{-1}).
C_{r}	rock (porosity) compressibility (Pa^{-1}).
C_{t}	total compressibility (Pa^{-1}).
C_β	non-Darcy flow constant ($\mathrm{m}^{3/2}$).
d_i	distance to the interface from gridblock i a (m).
D_i	depth to the center of gridblock i (m).
F_{f}	mass flux of fluid f ($\mathrm{kg\,s^{-1}}$).
$g, \mathbf{g}$	gravitational constant ($\mathrm{m\,s^{-2}}$).
h	thickness of formation (m).
k	absolute permeability (m^2).
k_{F}	fracture permeability (m^2).
k_{M}	matrix permeability (m^2).
k_{rf}	relative permeability to phase f.

l	average linear distance for fracture/matrix flow with the double-porosity model (m).
l_{FM}	characteristic distance for calculating fracture/matrix flow with the double-porosity model (m).
P	pressure (Pa).
P_{cgn}	gas–NAPL capillary pressure (Pa).
P_{cgw}	gas–water capillary pressure (Pa).
P_{cnw}	NAPL–water capillary pressure (Pa).
P_{D}	dimensionless pressure.
P_{g}	gas pressure (Pa).
P_{n}	NAPL pressure (Pa).
P_{w}	water pressure (Pa).
Q_{f}	mass sink/source term (kg s^{-1}).
R^{f}	mass residual term (kg s^{-1}).
q_{f}	mass sink/source term (kg s^{-1} m^{3}).
q_{m}	mass injection rate (kg s^{-1}).
q_{v}	volumetric injection rate (m^{3} s^{-1}).
S_{g}	gas pressure.
S_{n}	NAPL pressure.
S_{w}	water pressure.
x_{m}	primary variables to residual equations.
r	radial distance (m).
r_{D}	dimensionless radius.
r_e	outer boundary radius (m).
r_{w}	wellbore radius (m).
t	time (s).
t_{D}	dimensionless time, Equation (6.2).
$\mathbf{v}$	Darcy or volumetric flow velocity (m s^{-1}).
v_{r}	radial Darcy or volumetric flow rate (m s^{-1}).
V_i	volume of gridblock i (m^{3}).
β, β_{f}	non-Darcy flow coefficient of fluid f (m^{-1}).
β_{D}	dimensionless non-Darcy flow coefficient.
$\beta_{\mathrm{D,f}}, \beta_{\mathrm{D,m}}$	dimensionless non-Darcy flow coefficients for fracture and matrix, respectively.
γ_{ij}	transmissivity between gridblocks i and j (kg m^{-3}).
λ_{f}	mobility of fluid f (Pa $\bullet$ s)$^{-1}$.
μ_{f}	viscosity of fluid f (Pa $\bullet$ s).
ρ_{f}	density of fluid f (kg m^{-3}).
ρ_{i}	initial or reference fluid density (kg m^{-3}).
ϕ	porosity.
ϕ_{i}	initial or reference porosity.
Ψ_{f}	flow potential term (Pa).

1. Introduction

Darcy's law of flow (or Darcy flow), describing a linear relationship between volumetric flow rate (Darcy velocity) and pressure (head or potential) gradient, has been the fundamental principle in flow and transport processes in porous media (Muskat, 1946). Any deviations from this linear relation may be defined as non-Darcy flow. In this work our concern is only with the non-Darcy flow caused by

high flow velocities. Even though Darcy's law has been used nearly exclusively in the studies of porous-medium phenomena, there is considerable evidence that high-velocity non- Darcy flow occurs in many subsurface systems, such as in the flow near wells of oil or gas production, water pumping, and liquid waste injection.

The effects of non-Darcy or high-velocity flow regimes in porous media have been observed and investigated for decades (e.g. Tek *et al.*, 1962; Scheidegger, 1972; Katz and Lee, 1990). However, theoretical, field and experimental studies performed so far on non-Darcy flow in porous media have focused mostly on single-phase-flow conditions that pertain to the oil and gas industry (Swift and Kiel, 1962; Tek *et al.*, 1962; Lee *et al.*, 1987). Some investigations have been conducted for non-Darcy flow in fractured reservoirs (Skjetne *et al.*, 1999) and for non-Darcy flow into highly permeable fractured wells (Guppy *et al.*, 1981, 1982). Other studies have concentrated on finding and validating correlations of non-Darcy flow coefficients (Liu *et al.*, 1995).

In studies of non-Darcy flow through porous median, the *Forchheimer* equation is generally used to describe single-phase non-Darcy flow. Several studies reported in the literature extend the *Forchheimer* equation to multiphase flow and provide equations for correlating non-Darcy flow coefficients under multiphase conditions (Evans *et al.*, 1987; Evans and Evans, 1988; Liu *et al.*, 1995). A recent study (Wang and Mohanty, 1999) has discussed the importance of multiphase non-Darcy flow in gas-condensate reservoirs and presents a pore-scale network model for describing non-Darcy gas-condensate flow. Because of insufficient study in this area as well as the mathematical difficulty in handling highly nonlinear, non-Darcy flow terms in multiphase flow equations, our understanding of non-Darcy flow through porous media is currently very limited.

The objective of this study is to develop a numerical method for modeling single-phase and multiphase non-Darcy flow through heterogeneous porous and fractured rocks. The model formulation incorporates the *Forchheimer* equation, based on an integral finite-difference or a control volume numerical discretization scheme. The proposed model formulation is implemented into a three-dimensional, three-phase flow simulator and is applicable to both single-porosity porous media and fractured rocks. For flow in a fractured medium, fracture-matrix interactions are handled using an extended dual-continuum approach, such as double- or multiple-porosity, or dual-permeability methods.

This paper discusses the model formulation and the numerical schemes implemented for modeling non-Darcy flow in porous media. The numerical scheme has been verified by comparing its results against those of analytical methods. As applications, numerical solutions are used to obtain some insight into the physics of flow involving non-Darcy flow effects in reservoirs. Furthermore, several type curves and analytical solutions are provided well-test analysis of non-Darcy flow to demonstrate the proposed methodology for modeling this type of flow in porous and fractured rocks.

2. Governing Equations

A multiphase system in a porous or fractured aquifer is assumed to be composed of three phases: NAPL (oil), gas (air), and water. For simplicity, the three fluid components, water, NAPL, and gas, are assumed to be present only in their associated phases. Each phase flows in response to pressure, gravitational, and capillary forces according to the multiphase extension of Darcy's law for Darcy flow and the *Forchheimer* equation for non-Darcy flow. In an isothermal system containing three mass components, three mass-balance equations are needed to fully describe the system, as described in an arbitrary flow region of a porous or fractured domain.

For flow of phase f (f = w for water, f = n for NAPL or oil, and f = g for gas),

$$\frac{\partial}{\partial t}(\phi\, S_{\mathrm{f}}\, \rho_{\mathrm{f}}) = -\nabla \bullet (\rho_{\mathrm{f}} \mathbf{v}_{\mathrm{f}}) + q_{\mathrm{f}} \tag{2.1}$$

where ρ_f is the density of fluid f; $\mathbf{v}_{\mathrm{f}}$ is the Darcy (or volumetric) velocity of fluid f; S_{f} is the saturation of fluid f; ϕ is the effective porosity of formation; t is time; and q_{f} is the sink/source term of phase (component) f per unit volume of formation, representing mass exchange through injection/production wells or due to fracture and matrix interactions.

Volumetric flow rate (namely Darcy velocity for Darcy flow) for non-Darcy flow of each fluid may be described using the multiphase extension of the *Forchheimer* equation (Evans and Evans, 1988; Liu *et al.*, 1995)

$$-(\nabla P_{\mathrm{f}} - \rho_{\mathrm{f}} \mathbf{g}) = \frac{\mu_{\mathrm{f}}}{k_{\mathrm{rf}}} k \mathbf{v}_{\mathrm{f}} + \beta_{\mathrm{f}} \rho_{\mathrm{f}} \mathbf{v}_{\mathrm{f}} |\mathbf{v}_{\mathrm{f}}|, \tag{2.2}$$

where P_{f} is the pressure of phase f; $\mathbf{g}$ is the gravitational constant vector; k is the absolute/intrinsic permeability of the formation; k_{rf} is relative permeability to phase f; and β_{f} is the effective non-Darcy flow coefficient with a unit m^{-1} for fluid f under multiphase flow conditions (Evans and Evans, 1988).

Under single-phase flow conditions the coefficient, β_{f}, is traditionally called a turbulence coefficient or an inertial resistance coefficient (Tek *et al.*, 1962; Lee *et al.*, 1987). Note that to include multiphase effects on non-Darcy flow, Equation (2.2) has been modified by the following:

- Pressure gradient is replaced by flow potential gradient (the left-hand side term of (2.2)) to include gravity effects.
- Absolute permeability is replaced by an effective permeability term ($k\, k_{\mathrm{rf}}$).
- β_{f} is described as the effective non-Darcy flow coefficient for a flowing phase under multiphase flow conditions.

Darcy's law states that a linear relationship exists between volumetric flow rate and pressure (head or potential) gradient in porous media. The linear term, the first term ($(\mu_{\mathrm{f}}/k k_{\mathrm{rf}})\, \mathbf{v}_{\mathrm{f}}$) on the right-hand side of Equation (2.2), represents viscous flow; it is dominant at low flow rates. The additional pressure drop or energy assumption

resulting from non-Darcy or high flow velocities is described by the second term ($\beta_f \rho_f \mathbf{v}_f |\mathbf{v}_f|$) on the right-hand side of (2.2) for the extra friction or inertial effects (Katz and Lee, 1990). Equation (2.2) indicates that the non-Darcy flow equation reduces to the multiphase Darcy law if the non-Darcy term ($\beta_f \rho_f \mathbf{v}_f |\mathbf{v}_f|$) can be ignored, when compared with the first term ($(\mu_f / k k_{rf})\, \mathbf{v}_f$), at low flow velocity, Equation (2.2) becomes Darcy's law. For high velocities, however, the second term becomes dominant and must be included. Therefore, Darcy flow can generally be considered as a special case of non-Darcy flow, as described by Equation (2.2).

Equation (2.2) implicitly defines the Darcy velocity as a function of pressure gradient as well as saturation and relative permeability. A more general relation for the Darcy velocity in multiphase non-Darcy flow may be proposed as a function of pressure gradient, saturation, and relative permeability functions

$$\mathbf{v}_f = \mathbf{v}_f(\nabla P_f, S_f, k_{rf}). \tag{2.3}$$

With Equation (2.3), many other kinds of equations for non-Darcy flow in addition to the *Forchheimer* equation (e.g. Scheidegger, 1972) can be extended to multiphase non-Darcy flow situations.

Equation (2.1), the governing of mass balance for three phases, needs to be supplemented with constitutive equations, which express all the secondary variables and parameters as functions of a set of primary thermodynamic variables of interest. The following relationships will be used to complete the description of multiphase flow through porous media:

$$S_w + S_n + S_g = 1. \tag{2.4}$$

The capillary pressures relate pressures between the phases. The aqueous- and gas-phase pressures are related by

$$P_w = P_g - P_{cgw}(S_w), \tag{2.5}$$

where P_{cgw} is the gas–water capillary pressure in a three-phase system and assumed to be a function of water saturation only. The NAPL pressure is related to the gas phase pressure by

$$P_n = P_g - P_{cgn}(S_w, S_n), \tag{2.6}$$

where P_{cgn} is the gas–NAPL capillary pressure in a three-phase system, which is a function of both water and NAPL saturations. For many aquifer formations, the wettability order is (1) aqueous phase, (2) NAPL phase, and (3) gas phase. The gas–water capillary pressure is usually stronger than the gas–NAPL capillary pressure. In a three-phase system, the NAPL–water capillary pressure, P_{cnw}, may be defined as

$$P_{cnw} = P_{cgw} - P_{cgn} = P_n - P_w. \tag{2.7}$$

The relative permeabilities are assumed to be functions of fluid saturations only. The relative permeability to the water phase is taken to be described by

$$k_{\mathrm{rw}} = k_{\mathrm{rw}}(S_{\mathrm{w}}) \tag{2.8}$$

to the NAPL phase by

$$k_{\mathrm{rn}} = k_{\mathrm{rn}}(S_{\mathrm{w}}, S_{\mathrm{g}}) \tag{2.9}$$

and to the gas phase by

$$k_{\mathrm{rg}} = k_{\mathrm{rg}}(S_{\mathrm{g}}). \tag{2.10}$$

The densities of water, NAPL, and gas, as well as the viscosities of fluids, can in general be treated as functions of fluid pressures.

3. Numerical Formulation

The multiphase non-Darcy flow equations, as discussed in Section 2, have been implemented into a general-purpose, three-phase reservoir simulator, the MSFLOW code (Wu, 1998). As implemented in the code, Equation (2.1) can be discretized in space using an integral finite-difference or control-volume finite-element scheme for a porous and/or fractured medium. The time discretization is carried out with a backward, first-order, finite-difference scheme. The discrete nonlinear equations for water, NAPL, and gas flow at Node i are written as follows:

$$\{(\phi\, S_{\mathrm{f}}\, \rho_{\mathrm{f}})_i^{n+1} - (\phi\, S_{\mathrm{f}}\, \rho_{\mathrm{f}})_i^{n}\}\frac{V_i}{\Delta\, t} = \sum_{j\,\in\,\eta_i} F_{\mathrm{f}})_{i\,j}^{n+1} + Q_{\mathrm{f}\,i}^{n+1} \tag{3.1}$$

where n denotes the previous time level; $n+1$ is the current time level; V_i is the volume of element i (porous or fractured block); Δt is the time step size; η_i contains the set of neighboring elements (j), porous or fractured block, to which element i is directly connected; and F_{f} is a mass flow term between elements i and j, defined (when Equation (2.2) is used) as

$$F_{\mathrm{f}} = \frac{A_{ij}}{2(k\beta_{\mathrm{f}})_{ij+1/2}}\left\{-\frac{1}{\lambda_{\mathrm{f}}} + \left[\left(\frac{1}{\lambda_{\mathrm{f}}}\right)^2 - \gamma_{ij}(\psi_{\mathrm{f}j} - \psi_{\mathrm{f}i})\right]^{1/2}\right\}, \tag{3.2}$$

where subscript $ij+1/2$ denotes a proper averaging of properties at the interface between the two elements and A_{ij} is the common interface area between connected elements i and j. The mobility of phase f is defined as

$$\lambda_{\mathrm{f}} = \frac{k_{\mathrm{rf}}}{\mu_{\mathrm{f}}} \tag{3.3}$$

and the flow potential term is

$$\psi_{\mathrm{f}i} = P_{\mathrm{f}i} - \rho_{ij+1/2}\mathrm{g}D_i, \tag{3.4}$$

where D_{i} is the depth to the center of element i. The mass sink/source term at element i, $Q_{\mathrm{f}i}$ for phase f, is defined as

$$Q_{\mathrm{f}\,i} = q_{\mathrm{f}i}\, V_i. \tag{3.5}$$

In (3.2), transmissivity of flow terms is defined (if the integral finite-difference scheme is used) as,

$$\gamma_{ij} = \frac{4(k^2 \rho_{\mathrm{f}} \beta_{\mathrm{f}})_{ij+1/2}}{d_i + d_j}, \tag{3.6}$$

where d_i is the distance from the center of element i to the interface between elements i and j.

In the model formulation, absolute permeability, relative permeability and the effective non-Darcy flow coefficient are all considered as flow properties of the porous media and need to be averaged between connected elements in calculating the mass flow terms. In general, weighting approaches used are that absolute permeability is harmonically weighted along the connection between elements i and j, relative permeability and non-Darcy flow coefficients are both upstream weighted.

Newton/Raphson iterations are used to solve Equation (3.1). For a three-phase flow system, $3 \times N$ coupled nonlinear equations must be solved (N being the total number of elements of the grid), including three equations at each element for the three mass-balance equations of water, NAPL, and gas, respectively. The three primary variables (x_1, x_2, x_3) selected for each element are gas pressure, gas saturation, and NAPL saturation, respectively. In terms of the three primary variables, the Newton/Raphson scheme gives rise to

$$\sum_m \frac{\partial\, R_i^{\beta,\, n+1}(x_{m,\, p})}{\partial\, x_m}(\delta x_{m,\, p+1}) = -R_i^{\beta,\, n+1}(x_{m,\, p}) \quad \text{for} \quad m = 1, 2, 3, \tag{3.7}$$

where index $m = 1, 2$, and 3 indicates the primary variable 1, 2, or 3, respectively; p is the iteration level; and $i = 1, 2, 3, \ldots, N$, the nodal index. The primary variables are updated after each iteration

$$x_{m,\, p+1} = x_{m,\, p} + \delta x_{m,\, p+1}. \tag{3.8}$$

A numerical method is used to construct the Jacobian matrix for Equation (3.7), as outlined by Forsyth *et al.* (1995).

Similarly to Darcy flow, first-type or Dirichlet boundary conditions denote constant or time-dependent phase pressure, and saturation conditions. These types of boundary conditions can be treated using the large-volume or inactive-node method (Pruess, 1991), in which a constant pressure/saturation node may be specified with a huge volume while keeping all the other geometric properties of the mesh unchanged. However, caution should be taken in (1) identifying phase conditions when specifying the 'initial condition' for the large-volume boundary node and (2) distinguishing upstream/injection from downstream/production nodes. Once

specified, primary variables will be fixed at the big-volume boundary nodes, and the code handles these boundary nodes exactly like any other computational nodes.

Flux-type or Neuman boundary conditions are treated as sink/source terms, depending on the pumping (production) or injection condition, which can be directly added to Equation (3.1). This treatment of flux-type boundary conditions is especially useful for a situation where flux distribution along the boundary is known, such as dealing with a single-node well. More general treatment of multilayered well-boundary conditions is discussed in Wu (2000a).

4. Handling Non-Darcy Flow in Fractured Media

The technique used in the current model for handling non-Darcy flow through fractured rock follows the dual-continuum methodology (Warren and Root, 1963; Pruess and Narasimhan, 1985; Pruess, 1991). The method treats fracture and matrix flow and interactions using a multi-continuum numerical approach, including the double- or multiporosity method (Wu and Pruess, 1988), the dual-permeability method, and the more general 'multiple interacting continua' (MINC) method (Pruess and Narasimhan, 1985).

Since the 1960's, significant progress has been made in understanding and modeling fracture flow phenomena in porous media (e.g. Barenblatt *et al.*, 1960; Warren and Root, 1963; Kazemi, 1969; Pruess and Narasimhan, 1985). The classical double-porosity concept for modeling flow in fractured porous media, as developed by Warren and Root (1963), is physically based, which assumes that a flow domain is composed of matrix blocks of low permeability, embedded in a network of interconnected, more permeable fractures. Global flow in the formation occurs only through the fracture system, described as an effective porous continuum. The matrix behaves as spatially distributed sinks or sources to the fracture system without accounting for global matrix-matrix flow. If a global matrix-matrix flow is included, the approach becomes a dual-permeability conceptual model. The double-porosity or dual-permeability model relies on a quasi-steady-state flow assumption to account for fracture-matrix interflow. This may limit their applicability in application to situations having only matrix blocks of small size to satisfy the quasi-steady state mass transfer condition. Some recent studies present more rigorous mathematical derivations of the double-porosity model and therefore provide better understanding into interactions between the overlapping fracture/matrix systems for both single-phase and two-phase flow (Douglas, 1989; Arbogast, 1993; Douglas *et al.*, 1993).

As discussed above, one of the major limitations of the Warren–Root double-porosity model is the quasi-steady-state fracture/matrix assumption. This limitation has been removed in an improved model of Lai *et al.* (1983). They couple fracture/matrix interaction along matrix surfaces using the continuity condition in pressure and mass exchange rate analytically for given size (cube) matrix blocks. Numerically, on the other hand, it is much easier to handle fracture/matrix interac-

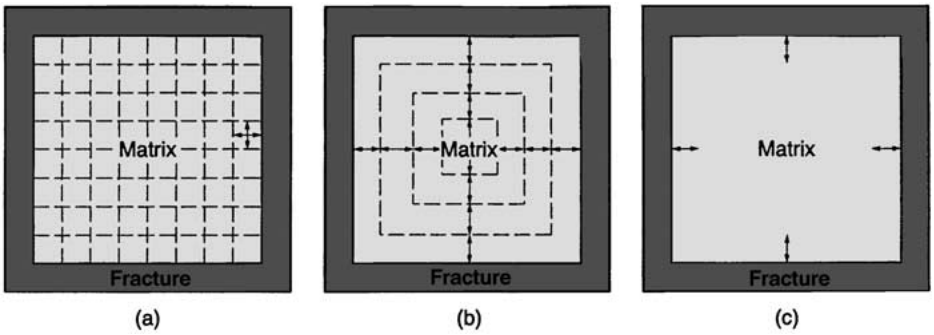

Figure 1. Schematic of different discretizations of cubic matrix blocks by the MINC concept: (a) explicit discretization; (b) nested discretization; (c) double-porosity discretization.

tions rigorously, because no quasi-steady-state assumption is needed. The generalized dual-continuum method, such as the MINC concept (Pruess and Narasimhan, 1985) and the multiporosity model (Wu and Pruess, 1988), can describe flow in a fracture/matrix system with any size and shape of matrix blocks and with fully transient handling of fracture/matrix interactions. The generalized dual-continuum, MINC method, can handle any flow processes of fractured media with matrix size varying from as large as the model domain of interest to as small as a representative elementary volume (REV) of zero volume. In general, the fracture network can be continuous in a pattern, randomly distributed or discrete.

For demonstration, Figure 1 presents several commonly used conceptual models of numerical discretization for handling fracture/matrix flow and interactions with the dual-continuum approach. Here we use a cubic shape as an example. Figure 1(a) shows a detailed, explicit discretized mesh for representing the matrix block of any size. If needed, this type of MINC discretization can be used to study heterogeneity within both matrix and fractures (by subdividing fractures into a number of segments) and to cover discrete fracture models. Of course, computational requirements may be intensive because a large number of grid blocks are often encountered with such discretization. The second MINC concept, as shown in Figure 1 (b), describes gradients of pressures and saturations between fractures and matrix by appropriate, nested subgridding of the matrix blocks. This approach provides a better approximation for transient fracture-matrix interactions than using the quasi-steady-state flow assumption of the Warren and Root model and at the same time results in better numerical performance then the explicit discretization. This model is the basic concept of MINC (Pruess and Narasimhan, 1985), which is based on the assumption that changes in fluid pressures and fluid saturations will propagate rapidly through the fracture system, while only slowly invading the tight matrix blocks. Therefore, changes in matrix conditions will be controlled locally by the distance to the fractures. Fluid flow between fractures and matrix blocks can then be modeled by means of one-dimensional strings of nested grid blocks. The accuracy of this nested discretization depends on the one-dimensional flow

approximation within matrix blocks, which may in turn depend on matrix block size (Wu and Pruess, 1988).

As a special case of the MINC concept, the classical double-porosity or the dual permeability model, as shown in Figure 1(c), approximates fracture and matrix each by one gridblock and interconnecting between them. Because of the one block representation of fractures or matrix, the interflow between fractures and matrix has to be handled using some quasi-steady-state flow assumption, as used with the Warren and Root model. Also, because the matrix is approximated using a single gridblock, the ability to evaluate gradients of pressures, saturation and capillary pressures within matrix will be limited. The accuracy of the discretization depends in general on matrix block size as well as matrix permeability and capillary properties for handling multiphase flow and interactions (Wu and Pruess, 1988). However, a very attractive advantage with the double-porosity approach is its computational efficiency, compared with the other two discretizations. Therefore, the double-porosity method has been the most widely used modeling approach in application.

The non-Darcy flow formulation, Equations (2.1) and (3.1), as discussed above, is applicable to both single-continuum and multi-continua media. Using the dual-continuum concept, Equations (2.1) and (3.1) can be used to describe single-phase and multiphase flow, respectively, both in fractures and inside matrix blocks when dealing with fractured reservoirs. A special attention needs to be paid to treating fracture/matrix flow terms with Equations (3.1) and (3.2) for estimation of mass exchange at fracture/matrix interfaces using a double-porosity approach. In particular, Appendix B shows that the characteristic length of non-Darcy flow distance between fractures and matrix crossing the interface for the double-porosity or the nested discretizations may be approximated using the results for Darcy flow (Warren and Root, 1965; Pruess, 1983). The flow between fractures and matrix is still evaluated using Equation (3.2), however, the transmissivity for the fracture/matrix flow is then given by

$$\gamma_{ij} = \frac{4(k_{\mathrm{M}}^2 \rho_{\mathrm{f}} \beta_{\mathrm{f}})_{ij+1/2}}{l_{\mathrm{FM}}}, \tag{4.1}$$

where l_{FM} is a characteristic distance for flow crossing fracture/matrix interfaces. For 1-D, 2-D and 3-D dimensions of rectangular matrix blocks, characteristic distances, based on quasi-steady flow assumption, are given in Table I.

When handling flow through a fractured rock using the numerical formulation of this work, the problem essentially becomes how to generate a mesh that represents both the fracture and matrix systems. Several fracture-matrix subgridding schemes exist for designing different meshes for different fracture-matrix conceptual models (Pruess, 1983). Once a proper mesh of a fracture-matrix system is generated, fracture and matrix blocks are specified to represent fracture or matrix domains, separately. Formally, they are treated in exactly the same way in the solution of the discretized model. However, physically consistent fracture and matrix

Table I. Characteristic distances for non-Darcy flow crossing fracture/matrix interfaces using the double-porosity and nested discretizations (Warren and Root, 1963; Pruess, 1983)

Case	Dimensions of matrix blocks[1]	Average linear distances (m)	Characteristic distance (m)
1-D	a	$l = a$	$l_{\mathrm{FM}} = \frac{l}{6}$
2-D	a b	$l = \frac{2ab}{a+b}$	$l_{\mathrm{FM}} = \frac{l}{8}$
3-D	a b c	$l = \frac{2abc}{a+b+c}$	$l_{\mathrm{FM}} = \frac{l}{10}$

[1] a, b and c are dimensions of matrix blocks along x, y and z coordinates, respectively, as defined by Warren and Root (1963).

properties and modeling conditions must be appropriately specified for fracture and matrix systems, respectively.

5. Model Verification

In this section we provide three examples to test and verify the proposed numerical schemes involved in handling non-Darcy flow of single-phase and multi-phase fluids in porous and fractured media. Several analytical solutions are used in these comparisons. The sample problems are:

- Single-phase, steady-state non-Darcy flow in homogenous porous media.
- Single-phase, transient non-Darcy flow through a double-porosity reservoir.
- Two-phase non-Darcy flow and displacement in a homogenous porous medium.

5.1. SINGLE-PHASE, STEADY-STATE RADIAL FLOW

This problem is used to verify the numerical scheme for modeling steady-state, non-Darcy flow in homogeneous porous media. For the comparative study, an exact analytical solution for this problem is presented in Appendix A. The test problem concerns steady-state, one-dimensional, and horizontal radial flow toward a well in a uniform and homogeneous system. A non-Darcy flow correlation from Tek *et al.* (1962) is used to evaluate the non-Darcy flow coefficient β versus porosity and permeability as follows:

$$\beta = \frac{C_\beta}{k^{5/4}\phi^{3/4}}, \tag{5.1}$$

Table II. Parameters for the steady-state single-phase flow problem

Parameter	Value	Unit
Reference pressure	$P_i = 10$	Bar
Reference porosity	$\phi_i = 0.20$	
Reference fluid density	$\rho_i = 1,000$	$kg\,m^{-3}$
Formation thickness	$h = 10$	m
Fluid Viscosity	$\mu = 1 \times 10^{-3}$	Pa • s
Fluid compressibility	$C_f = 5 \times 10^{-10}$	Pa^{-1}
Rock compressibility	$C_r = 5 \times 10^{-9}$	Pa^{-1}
Permeability	$k = 9.869 \times 10^{-13}$	m^2
Water production rate	$q_m = 0.1$	$kg\,s^{-1}$
Wellbore radius	$r_w = 0.1$	m
Outer boundary radius	$r_e = 1,000$	m
non-Darcy flow constant	$C_\beta = 3.2 \times 10^{-3}$, 3.2×10^{-4}, 3.2×10^{-9}	$m^{3/2}$

where C_β is a non-Darcy flow constant with a unit ($m^{3/2}$) when converted to SI units.

The numerical solution of this problem is performed by the multiphase flow code, MSFLOW, in which single-phase flow is handled as a special case of three-phase flow. A one-dimensional, radial-symmetric grid of 2,200 elements was generated along the 1,000 m of the radial flow direction. The parameters used for the comparison are listed in Table II for evaluating both analytical and numerical solutions. Comparisons of pressure distributions along the radial direction, calculated from the exact and numerical solutions, are shown in Figure 2. The agreement between the two solutions is excellent for different non-Darcy flow coefficients. In fact, many additional steady-state simulations have been performed and the numerical results are found to be in excellent agreement with the analytical solution in every case.

5.2. SINGLE-PHASE FRACTURED-MEDIUM FLOW PROBLEM

This problem tests the numerical formulation for simulating transient flow in fractured media by comparison with an analytical solution. The example concerns transient flow towards a well that fully penetrates a horizontal, uniform, fractured, radially infinite reservoir. When non-Darcy flow effects are small or can be ignored, the analytical solution by Warren and Root (1963) can be used for this particular test.

A radially symmetrical reservoir ($r = 5 \times 10^6$ m) is discretized into a one-dimensional (r), primary grid. The r-distance of 5×10^6 m is subdivided into 3,100

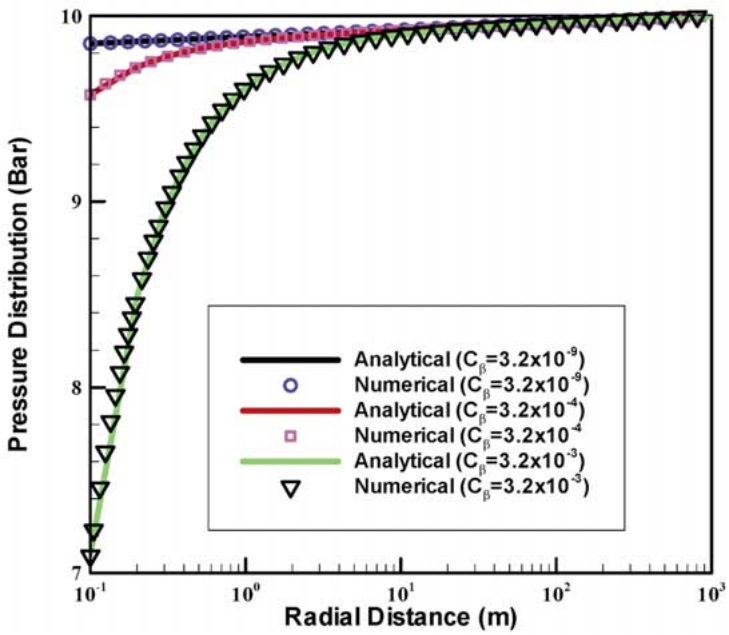

Figure 2. Comparison of dimensionless pressures calculated from exact and numerical solutions for steady-state non-Darcy flow with different non-Darcy flow coefficients.

intervals in logarithmic scale. A double-porosity mesh is generated from the primary grid, in which a three-dimensional fracture network and cubic matrix blocks are used. The matrix block size is $1 \times 1 \times 1$ m, and fracture permeability and aperture are correlated by the cubic law. Input parameters are given in Table III. Note that 10-times-larger non-Darcy flow coefficients than those for fractures are used correspondingly for flow in matrix to account for lower matrix permeability. A fully penetrating pumping well is represented by a well element with a specified constant water-pumping rate.

Figure 3 shows a comparison of the numerical modeling results and the Warren and Root solution for the pressure response at the well, in which the dimensionless variables were defined by Warren and Root (1963). Figure 3 shows that the simulated pressures at the well are in excellent agreement with the analytical solution, with a typical double-porosity behavior of two-parallel semi-log straight lines developed on the plot.

Figure 4 presents the simulation results including non-Darcy effects in both fracture-fracture and fracture-matrix flow, which is used to examines impact of non-Darcy flow between fracture and matrix systems in a double-porosity model. Figure 4 shows that non-Darcy flow between fractures and matrix has little effect on well pressures, even with non-Darcy flow coefficients of matrix rock increased by six orders of magnitude. Many additional simulations with different parameters have been performed for sensitivity analyses and all the results indicates flow

Table III. Parameters for the single-phase, fractured-medium flow problem

Parameter	Value	Unit
Matrix porosity	$\phi_M = 0.30$	
Fracture porosity	$\phi_F = 0.0006$	
Reference water density	$\rho_w = 1,000$	$kg\,m^{-3}$
Water phase viscosity	$\mu_w = 1 \times 10^{-3}$	Pa • s
Matrix permeability	$k_M = 1.0 \times 10^{-16}$	m^2
Fracture permeability	$k_F = 9.869 \times 10^{-13}$	m^2
Water production rate	$q_m = 0.1$	$kg\,s^{-1}$
Rock compressibility	$C_r = 1.0 \times 10^{-9}$	$1\,Pa^{-1}$
Water compressibility	$C_w = 5.0 \times 10^{-10}$	$1\,Pa^{-1}$
Dimensionless non-darcy Flow coefficient for fracture	$\beta_{D,f} = 1 \times 10^{-4}$, 1, 5, and 10	
Dimensionless non-Darcy Flow coefficient for matrix	$\beta_{D,m} = 1 \times 10^{-3}$, 10, 50, and 100	
Wellbore radius	$r_w = 0.1$	m

between fractures and matrix be effectively approximated as Darcy flow even flow through fractures are non-Darcy with a double-porosity concept.

5.3. TWO-PHASE NON-DARCY DISPLACEMENT

In this problem, an analytical solution (Wu, 2000b) is used to examine the validity of the numerical method for modeling multiphase non-Darcy flow and displacement processes. The *Forchheimer* equation is also used for the comparison. The physical flow model is a one-dimensional linear porous medium, which is at first saturated uniformly with a nonwetting fluid ($S_n = 0.8$) and a wetting fluid ($S_w = S_{wr} = 0.2$). A constant volumetric injection rate of the wetting fluid is imposed at the inlet ($x = 0$), starting from $t = 0$. The relative permeability curves used for all the calculations in this problem are shown in Figure 5, and rock and fluid properties are listed in Table IV.

In this problem, the effective non-Darcy flow coefficient for multiphase flow is treated as a function of fluid saturation and relative permeability. The non-Darcy flow coefficient correlation, defined by Equation (5.1), is extended to the two-phase flow situation with replacing the absolute permeability (k) by an effective permeability (kk_{rf}) and replacing porosity ϕ with $\phi(S_f - S_{fr})$. Then, we can derive the relationship for the non-Darcy flow coefficient as follows:

$$\beta_f(S_w, k_{rf}) = \frac{C_\beta}{(kk_{rf})^{5/4}[\phi(S_f - S_{fr})]^{3/4}}, \tag{5.2}$$

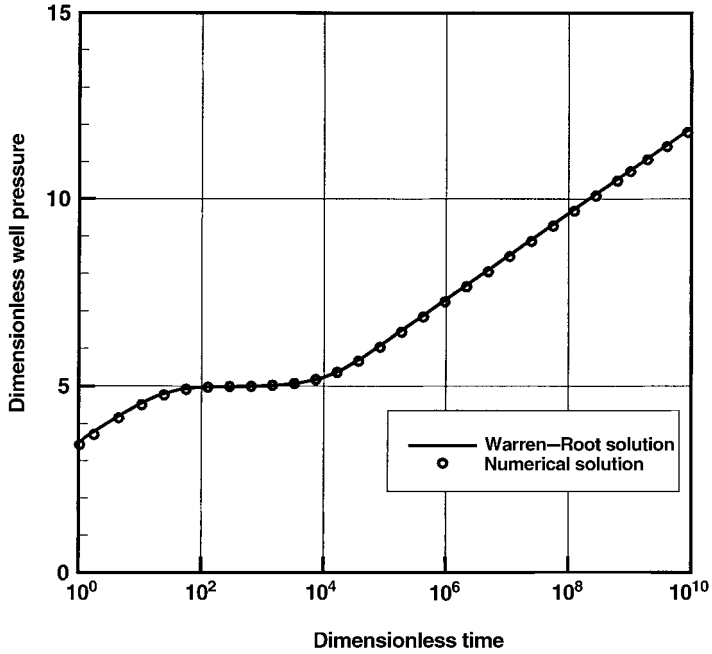

Figure 3. Comparison of dimensionless pressures calculated from analytical and numerical solutions for transient flow in double-porosity, fractured rock.

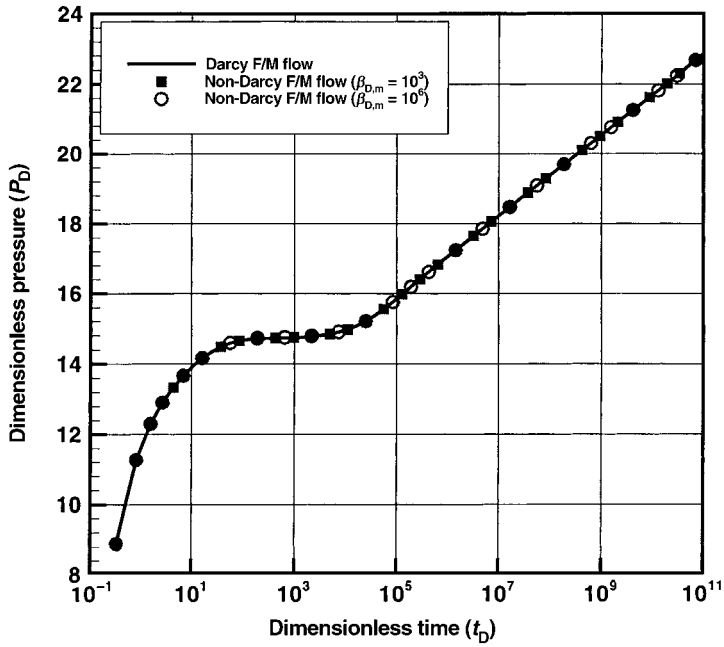

Figure 4. Effects of non-Darcy flow between fracture and matrix on dimensionless well pressures in double-porosity, fractured rock ($\beta_{D,f} = 10$).

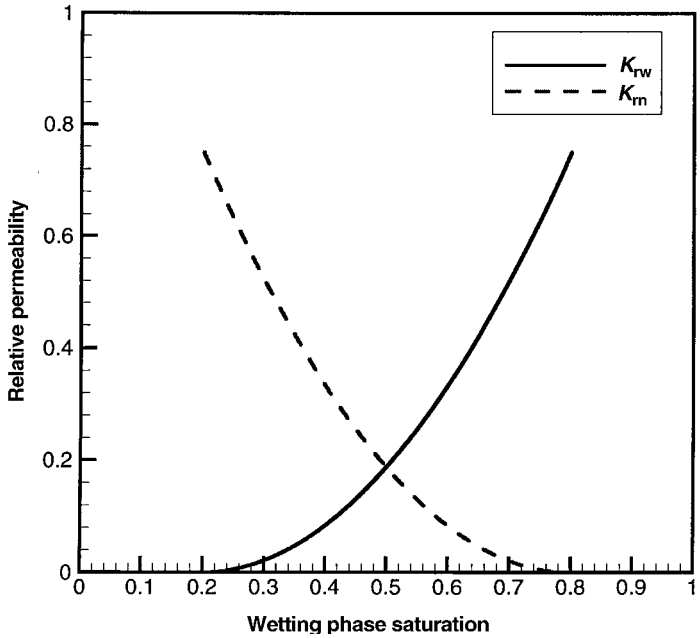

Figure 5. Relative-permeability curves used in analytical and numerical solutions for non-Darcy displacement.

Table IV. Parameters for the non-Darcy displacement example

Parameter	Value	Unit
Effective porosity	$\phi = 0.30$	
Permeability	$k = 9.869 \times 10^{-13}$	m^2
Wetting phase density	$\rho_w = 1,000$	$kg\,m^{-3}$
Wetting phase viscosity	$\mu_w = 1.0 \times 10^{-3}$	Pa • s
Nonwetting phase density	$\rho_n = 800$	$kg\,m^{-3}$
Nonwetting phase viscosity	$\mu_n = 5.0 \times 10^{-3}$	Pa • s
non-Darcy flow constant	$C_\beta = 3.2 \times 10^{-6}$	$m^{3/2}$
Injection rate	$q_v = 1.0 \times 10^{-5}$	$m^3\,s^{-1}$

where S_{fr} is residual saturation of fluid f. Equation (5.2) is incorporated into both the analytical and numerical calculations.

To reduce the effects of discretization on numerical simulation results, we choose very fine, uniform mesh spacing ($\Delta x = 0.01$ m). A one-dimensional 5 m linear domain is discretized into 500 one-dimensional uniform gridblocks. In the numerical simulation, the non-Darcy flow coefficient, Equation (5.2), is treated as a flow property and is evaluated using a full upstream weighting scheme such as that for the relative permeability function.

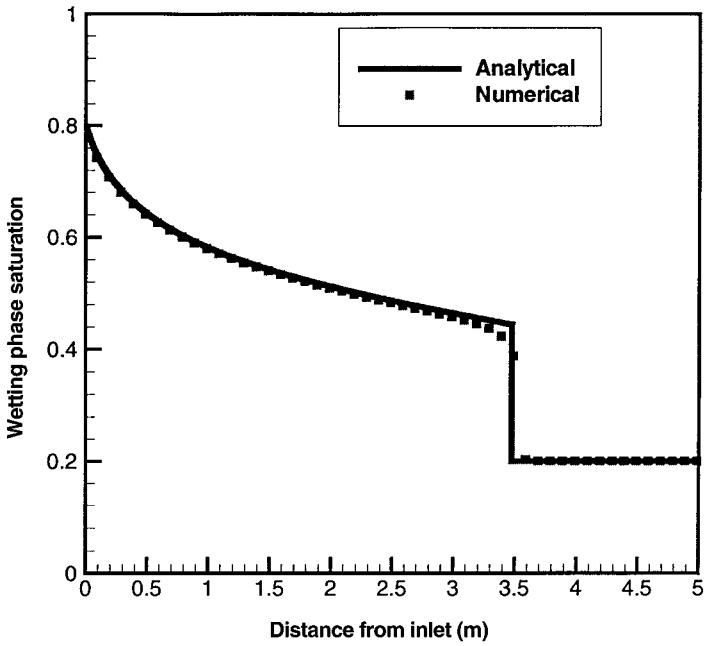

Figure 6. Comparison between saturation profiles calculated from analytical and numerical solutions after 10 h of injection.

Figure 6 shows saturation profiles after 10 h from both analytical and numerical solutions. The figure indicates that the numerical results are in excellent agreement with the analytical prediction of the non-Darcy displacement for the entire wetting-phase sweeping zone. Except at the shock, advancing saturation front, the numerical solution deviates only slightly from the analytical solution, resulting from a typical 'smearing front' phenomenon of numerical dispersion effects that occurs when matching the Buckley–Leverett solution using numerical results (Aziz and Settari, 1979).

6. Application and Discussion

In this section, we present several applications and discuss single-phase, non-Darcy flow behavior to demonstrate the applicability of the present modeling approach to field problems. The applications generate dimensionless pressures or type curves for non-Darcy-flow well-test analyses, including:

1. Pressure drawdown and buildup analyses.
2. Effects of finite boundaries of reservoirs.
3. Pressure draw-down in fractured reservoirs.
4. Pressure responses in partially penetrating wells of porous and fractured reservoirs.
5. Well test determination of non-Darcy flow coefficients.

The first four examples deal with single-phase slightly compressible fluid transient flow and in these cases the compressibility of fluids and rock is an important parameter. The last problem provides a technique for estimating non-Darcy flow coefficients using steady-state well tests.

Before further discussing these applications, we introduce several dimensionless variables for analyzing single-phase flow and well test results (Earlougher, 1977). Let us define the following group of dimensionless variables:

The dimensionless radius

$$r_{\mathrm{D}} = \frac{r}{r_{\mathrm{w}}}, \tag{6.1}$$

the dimensionless time

$$t_{\mathrm{D}} = \frac{kt}{\phi_i \mu C_t r_{\mathrm{w}}^2}, \tag{6.2}$$

the dimensionless non-Darcy flow coefficient

$$\beta_{\mathrm{D}} = \frac{k q_{\mathrm{m}} \beta}{2\pi r_{\mathrm{w}} h \mu}, \tag{6.3}$$

and the dimensionless pressure

$$P_{\mathrm{D}} = \frac{P_i - P}{\frac{q_v \mu}{2\pi k h}}. \tag{6.4}$$

In these notations, the subscript referring to a phase is ignored, r is radial distance (coordinate), r_{w} is wellbore radius, ϕ_{i} is the effective (or initial) porosity of formation at reference (initial) pressure ($P = P_{\mathrm{i}}$), C_{t} is total compressibility of fluid and rock, h is thickness of formation, q_{m} is mass production or injection rate, and q_{v} is volumetric production or injection rate. Note that the permeability k in (6.2) and (6.3) should be fracture permeability with a double-porosity model.

6.1. PRESSURE DRAWDOWN AND BUILDUP ANALYSES

This example presents a set of type curves for analyzing well tests of single-phase, slightly compressible non-Darcy fluid flow in an infinite-acting reservoir. The basic modeling parameters are summarized in Table V. Non-Darcy flow is considered to occur into a fully penetrating well (the case of partial penetration is presented in § 6.4) from an infinite-acting, homogeneous and isotropic, uniform and horizontal formation. Even though skin and wellbore storage effects are ignored in the results, they can easily be included if needed.

The infinite-acting reservoir is approximated by a one-dimensional, radially symmetrical reservoir in the numerical model with age outer boundary radius of

Table V. Parameters for the pressure drawdown and buildup analysis

Parameter	Value	Unit
Initial pressure	$P_i = 10$	Bar
Initial porosity	$\phi_i = 0.20$	
Reference fluid density	$\rho_i = 1,000$	$kg\,m^{-3}$
Formation thickness	$h = 10$	m
Fluid viscosity	$\mu = 1 \times 10^{-3}$	Pa • s
Fluid compressibility	$C_f = 5 \times 10^{-10}$	Pa^{-1}
Rock compressibility	$C_r = 5 \times 10^{-9}$	Pa^{-1}
Permeability	$k = 9.869 \times 10^{-13}$	m^2
Water pumping rate	$q_v = 0.1$	$m^3\,d^{-1}$
Wellbore radius	$r_w = 0.1$	m
Outer boundary radius	$r_e = \infty \approx 5] \times 10^6$	m
Dimensionless non-Darcy	$\beta_D = 1 \times 10^{-3}, 1, 10, 100$	
Flow coefficient	$1 \times 10^3, 1 \times 10^4, 1 \times 10^5$	

5×10^6 m, discretized into a one-dimensional grid of 3,100 gridblocks in logarithmic scale. Initially, the system is undisturbed and at constant pressure. A fully penetrating production well, represented by a well element, starts pumping at $t = 0$, specified at a constant water-pumping rate.

A set of type-curves for pressure drawdown, calculated by the numerical model in terms of dimensionless pressure versus dimensionless time, is shown in Figure 7. Figure 7 clearly indicates that the non-Darcy flow coefficient is a very important and sensitive parameter to the pressure drawdown curves. When non-Darcy flow coefficients are sufficiently large, they affect pressure transient behavior during both earlier and later times. Note that in the simulation, the non-Darcy flow coefficient is evaluated to be uncorrelated with other parameters. Figure 7 indicates that the non-Darcy flow coefficient can be effectively estimated using the type curves with the traditional type-curve matching approach. Note also that for small non-Darcy flow coefficients, pressure declines at the well during pumping are approaching those predicted by the Theis solution, as they should do. This results from the diminishing effect of non-Darcy flow with flow behavior now tending towards to Darcy flow regime.

Figure 8 presents simulated pressure drawdown and buildup curves, in which the well is pumped for 1 day only and then shut off. The well pressure variations during the entire pumping and shut-in period, as shown in Figure 8, indicate that pressure buildup is insensitive to the values of non-Darcy flow coefficients, as compared with drawdown in pumping periods. This is because of rapid reduction in flow velocity near the well after a well is shut off and non-Darcy flow effects become ineligible. Many additional modeling investigations have verified this observation. This indicates that pressure-buildup tests are not suitable for estima-

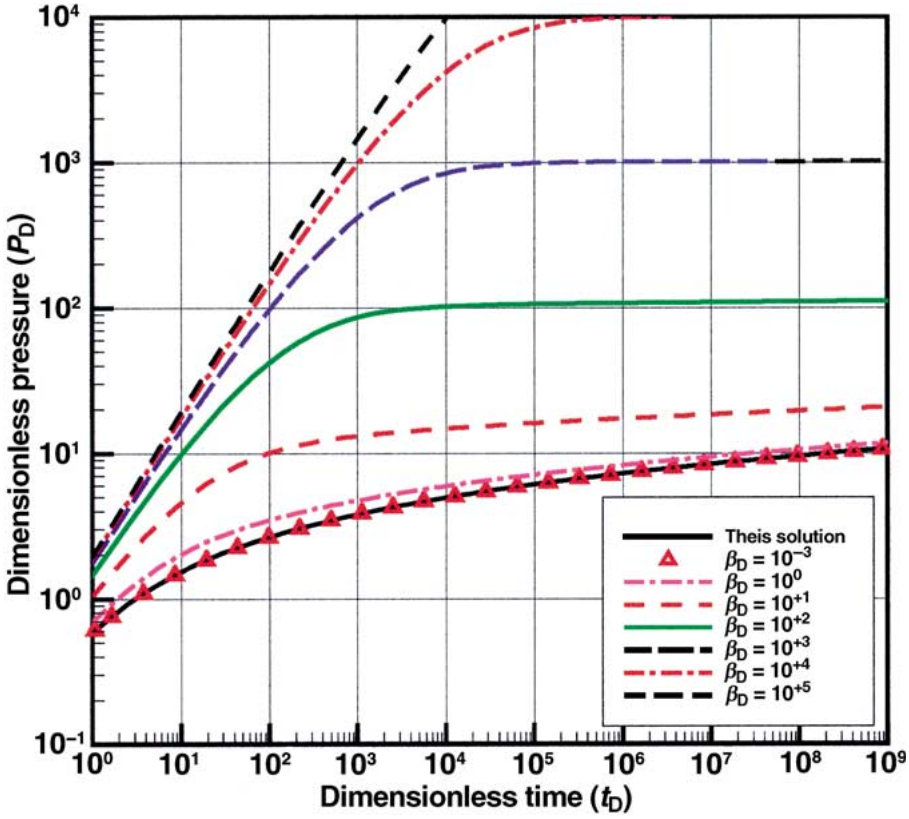

Figure 7. Type curves for dimensionless pressures for non-Darcy flow in an infinite system without wellbore storage and skin effects.

ting non-Darcy flow coefficients. On the other hand, the pressure-buildup method, following non-Darcy flow pumping tests, will be a good test for determining permeability values without significant non-Darcy flow.

6.2. EFFECTS OF FINITE RESERVOIR BOUNDARIES

For practical well tests, boundary effects or well interference in finite, developed reservoirs will show up sooner or later. Two types of boundary conditions, closed and constant pressure conditions, are commonly used to approximate the effects of finite reservoir/well boundaries. In this section, effects of finite-system boundary conditions on pressure drawdown behavior will be discussed.

The flow system and parameters for finite systems are similar to those in Section 6.1. Only two finite radial systems with outer boundary radii ($r_e = 1{,}000$ and 10,000 m) are considered. Figures 9 and 10 show dimensionless pressure drawdown curves, for closed and constant-pressure boundaries as well as the two radii. For a smaller formation system with $r_e = 1{,}000$ m, Figure 9 shows that significant

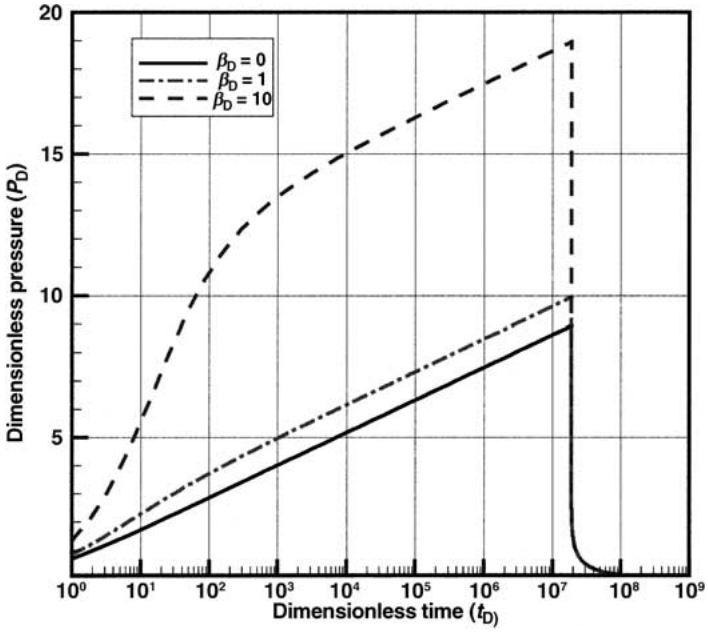

Figure 8. Dimensionless pressures for one-day pumping, followed by pressure buildup, of non-Darcy flow in an infinite system without wellbore storage and skin effects.

boundary effects occur at about dimensionless time $t_D = 10^8$ (1 day in real time), at which the well pressure responses deviate from the infinite-acting solution (say, the Theis solution for small non-Darcy flow coefficients). For the larger system with $r_e = 10{,}000$ m, boundary effects are very similar but show up much later (Figure 10).

6.3. ANALYSIS OF NON-DARCY FLOW IN FRACTURED MEDIA

This problem portrays non-Darcy flow through a fractured reservoir. The fracture-matrix formation is described using the Warren and Root double-porosity model. The physical flow model is the same as that in Section 5.2 for one-dimensional fracture-matrix system, with basic properties of rock and fluid also given in Table III.

For non-Darcy flow into a well from an infinite fractured system, well pressure type curves are shown in semi-log plots of Figure 11. The type curves on the figures show that well (fracture) pressures are extremely sensitive to the value of non-Darcy flow coefficients; therefore, well pumping tests will help to determine this constant in a fractured reservoir. Furthermore, Figure 11 indicates that the effects of non-Darcy flow on early transient pressure responses are very strong, such that the first semi-log straight lines may not develop when non-Darcy flow is involved.

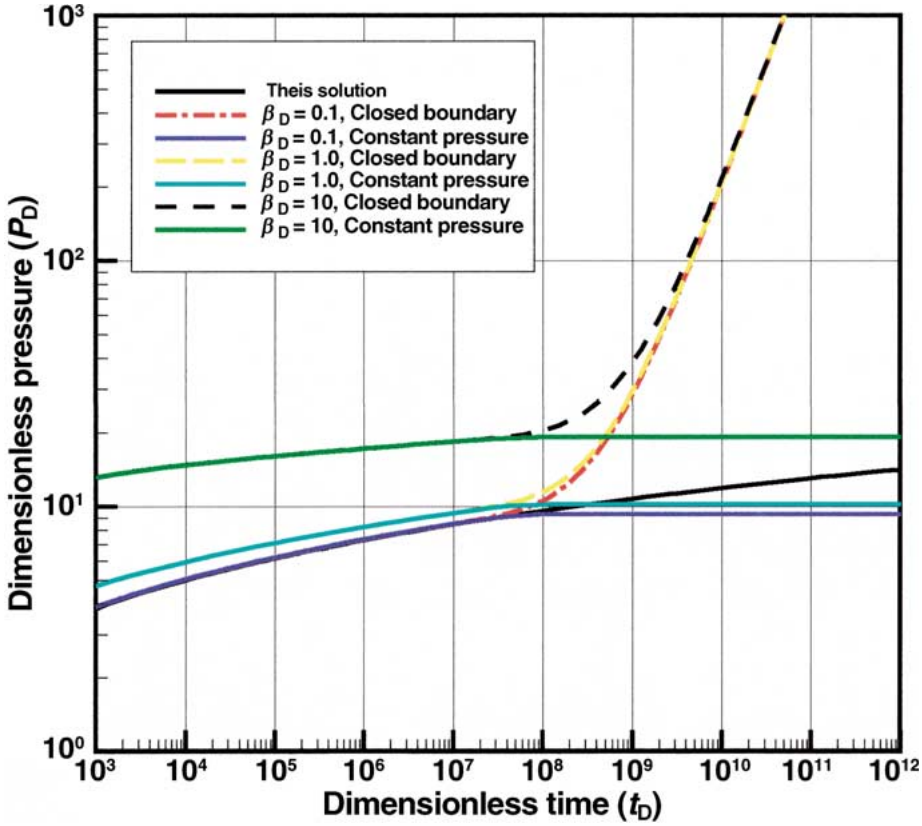

Figure 9. Type curves for dimensionless pressures for non-Darcy flow in a finite system with an outer boundary radius of 1,000 m.

6.4. NON-DARCY FLOW WITH PARTIAL PENETRATION AND PARTIAL COMPLETION

This section is to provide modeling results for analyzing well tests of non-Darcy fluid flow at a partially penetrating or completed well and also to present multi-dimensional flow modeling examples. Non-Darcy flow is considered to occur into a partially penetrating well from an infinite-acting, homogeneous and isotropic, porous or fractured reservoir. The flow near a partially penetrating production well is three-dimensional towards the wellbore and mathematically it is can be handled using a 2-D, axially-symmetrical $(r - z)$ grid.

The infinite-acting reservoir is approximated by a 2-D, radially symmetrical reservoir in the numerical model with an outer boundary radius ($r = 1 \times 10^7$ m) and a thickness of 10 m in the vertical, z-direction. The system is discretized into a 2-D grid of 1,000 divisions in the r direction using a logarithmic scale and five uniform grid layers in the z direction for the porous reservoir. For the fractured flow example, the single-porosity, porous reservoir grid is further processed into

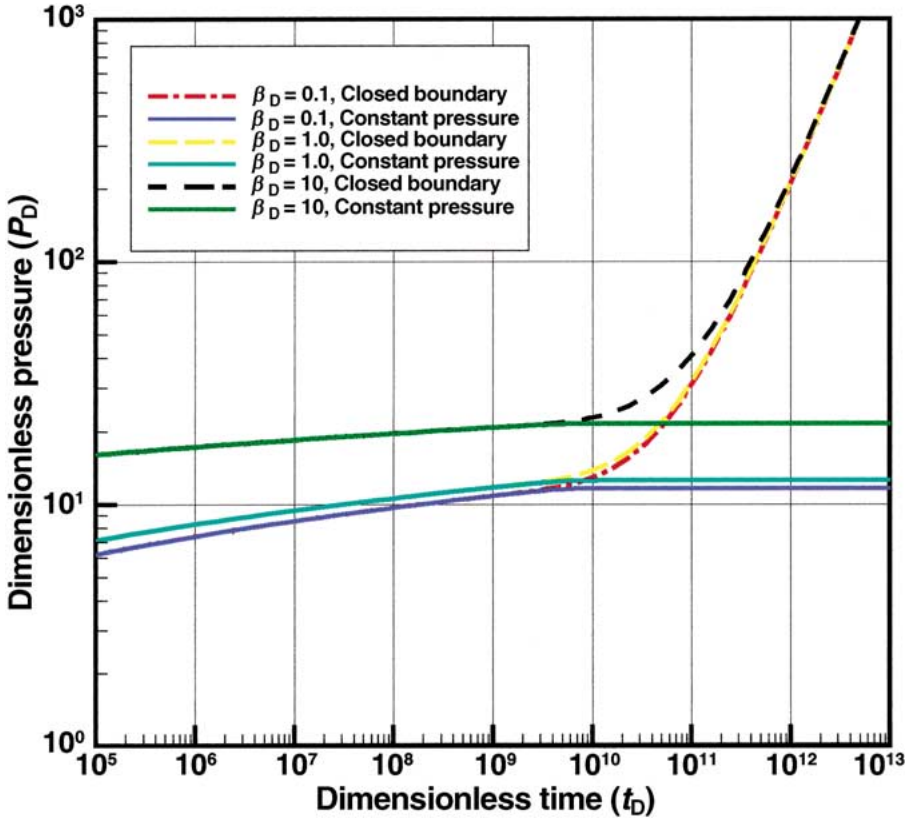

Figure 10. Type curves for dimensionless pressures for non-Darcy flow in a finite system with an outer boundary radius of 10,000 m.

a double-porosity grid using the MINC technology. Initially, the two single-phase systems are both at vertical-gravity equilibrium. Partially penetrating wells with percentage of wellbore completion are represented by single well elements and the results are compared.

The parameters for the porous medium reservoir are those as given in Table V and the fractured reservoir properties are given in Table III. The fractured reservoir is handled using the double-porosity model. Two type-curves for pressure drawdown, calculated in terms of dimensionless pressure versus dimensionless time, are shown in Figures 12 and 13, respectively, for the porous and fractured reservoirs. Figures 12 and 13 show a significant impact of percentage of well penetration on well pressure behavior in both the porous medium and fractured reservoirs. As completed well screen lengths decrease (i.e. wellbore penetration getting smaller), the flow resistance as well as pressure drops at the well increase significantly in order to maintain the same production rates. A larger impact of well partial penetration on non-Darcy flow regime near a well than on Darcy flow is expected, because of higher flow rates or large non-Darcy flow effects near wellbore. How-

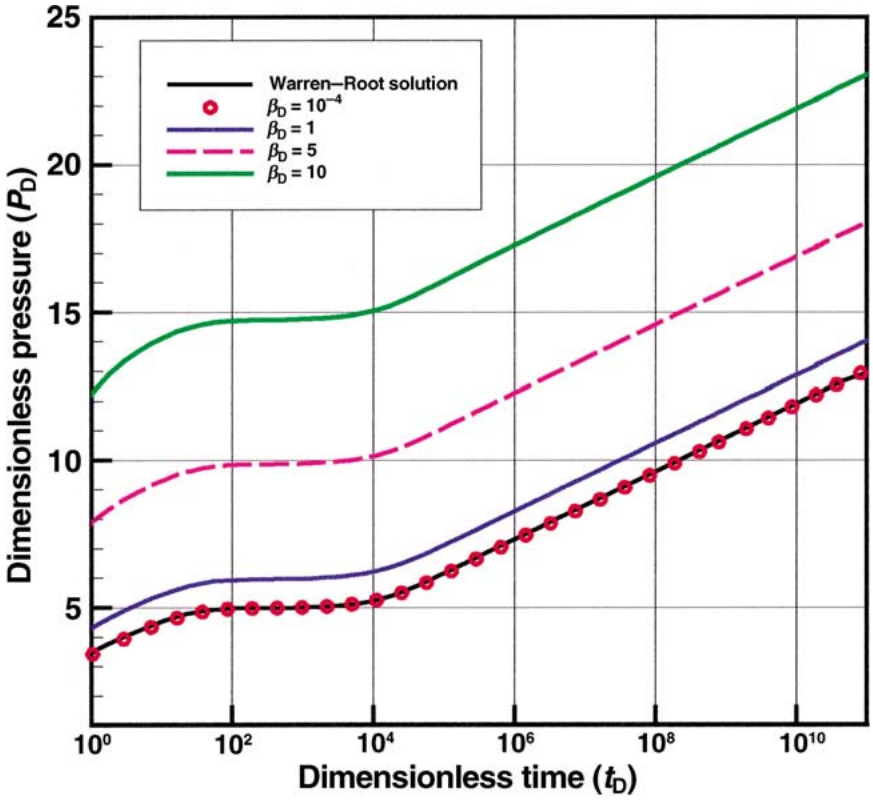

Figure 11. Type curves for dimensionless pressures for non-Darcy flow in an infinite fractured system without wellbore storage and skin effects.

ever, comparison of the straight lines developed in the type curves at late times (Figures 12 and 13) indicates that the same pseudo skin concept (Earlougher, 1977) may also be applicable to analyzing partial penetration effects of non-Darcy flow at wells.

6.5. DETERMINATION OF NON-DARCY FLOW COEFFICIENTS

In addition to the type-curve matching method for determining non-Darcy flow coefficients (as discussed above), we may derive a simpler approach. Type-curves observation in Figures 7–11 indicates that vertical displacement (difference in dimensionless pressures) at the same time between non-Darcy and Darcy flow solutions is always closely related to (dimensionless) non-Darcy flow coefficients as long as closed boundary effects are insignificant. A close examination of Figure 7 or 11 reveals

$$\Delta P_D \approx \beta_D \tag{6.5}$$

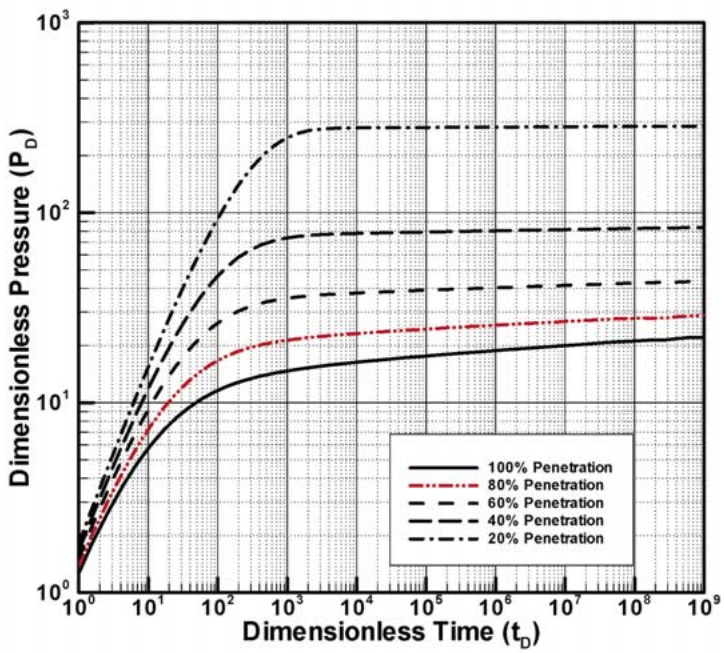

Figure 12. Type curves for dimensionless pressures of non-Darcy flow at partially penetrating wells in an infinite porous reservoir ($\beta_D = 10$) with different degrees of well penetration.

after the early transient times ($t_D = 10^5$ or 1,000 s in real time). Is this true? This can be further illustrated using a simple steady-state solution, provided in Appendix A. At steady-state and if $r_e \gg r_w$, the solution (A.15) becomes

$$P_D = \ln\left(\frac{r_D^e}{r_D}\right) + \beta_D\left(\frac{1}{r_D} - \frac{1}{r_D^e}\right) \approx \ln(r_D^e) + \beta_D, \tag{6.6}$$

at wells with $r = r_w$ or $r_D = 1$. The first term of (6.6), on the right-hand side, is identical to the solution for steady-state Darcy flow. Therefore, the difference in dimensionless pressure under steady state is approximately equal to a dimensionless non-Darcy flow coefficient, as defined in Equation (6.3). It is encouraging to note that this relation may provide a good approximation even for unsteady-state flow conditions after earlier transient periods, as shown in Figures 7–11.

The correlation of dimensionless non-Darcy flow coefficients with dimensionless pressures, as shown in Figure 7 and 11, as well as Equation (6.6), is equivalent to that of skin effects in a Darcy flow well-test analysis (Earlougher, 1977). This indicates that the non-Darcy flow effect is dominated mainly by the flow near the wellbore, because of the much higher flow velocities there. In general, skin and non-Darcy flow effects cannot be separated from a single well test under non-Darcy flow condition. We recommend that skin effects be estimated using a low flow rate or Darcy flow test first.

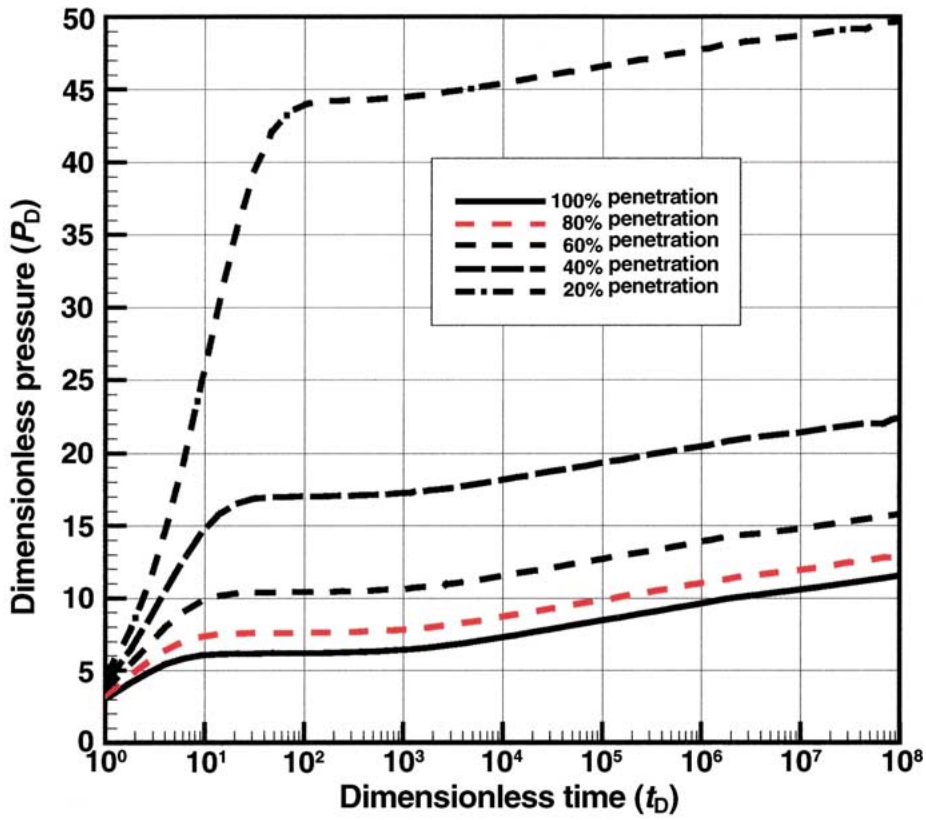

Figure 13. Type curves for dimensionless pressures of non-Darcy flow at partially penetrating wells in an infinite fractured reservoir ($\beta_D = 1$) with different degrees of well penetration.

Here, an example demonstrates how to use Equation (6.5) to determine non-Darcy flow coefficients by well tests. This simple method can be demonstrated using the simulated well test of Section 6.1. From the simulation, at $t_D = 0.1243 \times 10^8$ (or $t = 0.3778 \times 10^5$ s) the dimensionless well pressure $P_D = 18.53$ for $\beta_D = 10$, and $P_D = 8.52$ for $\beta_D = 0$. Substituting these dimensionless pressure difference data into Equation (5.6), together with the definition (6.3),

$$\begin{aligned} \beta &= \frac{\beta_D(2\pi r_w h\mu)}{kq_m} \approx \frac{\Delta p_D(2\pi r_w h\mu)}{kq_m} \\ &= \frac{(18.53 - 8.52) \times 2 \times \pi \times 10 \times 10^{-3}}{9.869 \times 10^{-13} \times 0.1} = 6.36 \times 10^{12}\,\mathrm{m}^{-1} \end{aligned} \tag{6.7}$$

The actual input value for β is 6.37×10^{12} in for the numerical test problem. The result indicates that the proposed well test method is very accurate for determining non-Darcy flow coefficients in this case.

7. Summary and Conclusions

This paper presents a numerical method and theoretical study for non-Darcy flow and displacement through porous and fractured media. The dual-continuum approach, commonly used for Darcy flow, is extended for handling non-Darcy flow in fractured formations. A three-dimensional, three-phase flow reservoir simulator has been enhanced to include the capability of modeling non-Darcy flow. Model formulation incorporates the *Forchheimer* equation to describe single-phase and multiphase non-Darcy flow. In addition, an analytical solution is derived for steady-state non-Darcy flow toward a well in a uniform radial flow system. The numerical scheme implemented has been verified by comparing numerical simulation results with those of analytical solutions under single-phase and multiphase, steady-state and transient flow conditions.

As applications, numerical as well as analytical solutions are used to obtain some insight into the physics of flow involving non-Darcy flow effects in porous media. The major findings of the work are as follows:

- Pressure drawdown not buildup behavior is sensitive to effects of non-Darcy flow, therefore pressure drawdown testing will be a more suitable approach for well-testing determination of non-Darcy flow coefficients.
- Non-Darcy flow coefficients can be effectively estimated using type-curve fitting methods or by steady-state flow tests. Several type curves for well testing analyses for flow through fully and partially penetrating wells in porous and fractured reservoirs are provided in this work along the methodology with steady-state testing technique.
- Well pressure responses of non-Darcy flow could be approximated using Darcy flow solutions, superposed only by a dimensionless non-Darcy flow coefficient (defined in this work), for flow problems in both single-porosity and double-porosity media. Therefore, many well testing analysis techniques, developed for Darcy flow, may be applicable for analyzing non-Darcy flow testing data.
- Non-Darcy flow effect lasts through the entire transient flow period during a well pumping or injection test and is equivalent to that of skin effects in a Darcy flow well-test analysis. Therefore the non-Darcy flow effect is dominated mainly by the flow near a wellbore and cannot be separated from the skin factor by a single well test under non-Darcy flow condition.

Appendix A. Steady-state Solution for Single-phase Flow

The steady-state flow problem considered here is fluid production from a fully penetrating well in a finite, radial system, subject to a constant outer boundary pressure.

$$\frac{\partial}{\partial r}[\rho(P) r v_{\mathrm{r}}] = 0, \tag{A.1}$$

where v_r is volumetric flow rate along the r-direction. At the outer boundary ($r = r_e$)

$$P(r = r_e) = P_i \quad \text{(constant)} \tag{A.2}$$

and at the inner boundary of the wellbore, $r = r_w$, the fluid is produced at a constant mass rate

$$2\pi r_w h[\rho v_r]_{r=r_w} = q_m \quad \text{(constant)} \tag{A.3}$$

Integrating Equation (A.1) leads to

$$[\rho(P) r v_r] = C \tag{A.4}$$

and using (A.3), we have

$$[\rho(P) r v_r] = \frac{q_m}{2\pi h}. \tag{A.5}$$

For the one-dimensional, horizontal, single-phase non-Darcy flow, v_r can be determined from Equation (2.2) as

$$v_r = \frac{1}{2k\rho\beta}\left\{-\mu + \left[\mu^2 + 4k^2\rho\beta\frac{\partial P}{\partial r}\right]^{1/2}\right\}. \tag{A.6}$$

We have

$$\frac{r}{2k\beta}\left\{-\mu + \left[\mu^2 + 4k^2\rho\beta\frac{\partial P}{\partial r}\right]^{1/2}\right\} = \frac{q_m}{2\pi h} \tag{A.7}$$

or

$$4k^2\rho\beta\frac{\partial P}{\partial r} = 2\mu\frac{kq_m\beta}{\pi h}\frac{1}{r} + \left(\frac{kq_m\beta}{\pi h}\frac{1}{r}\right)^2. \tag{A.8}$$

To solve Equation (A.8), we correlate the fluid density as a function of pressure

$$\rho = \rho(P) = \rho_i[1 + C_f(P - P_i)], \tag{A.9}$$

$$[1 + C_f(P - P_i)]\frac{\partial P}{\partial r} = \frac{q_v\mu}{2\pi kh}\frac{1}{r} + \frac{q_v\mu}{2\pi kh}\frac{kq_m\beta}{2\pi h\mu}\frac{1}{r^2}, \tag{A.10}$$

where $q_v = q_m/\rho_i$, is the volumetric production rate at the reference pressure. In terms of dimensionless variables

$$-[1 - Q_D P_D]\frac{\partial P_D}{\partial r_D} = \frac{1}{r_D} + \beta_D\frac{1}{r_D^2}, \tag{A.11}$$

where

$$Q_D = \frac{q_v\mu C_f}{2\pi kh}. \tag{A.12}$$

Finally, we have the steady-state solution

$$P_{\mathrm{D}} = \frac{1 - \left[1 - 2Q_{\mathrm{D}}\left(\ln\left(\frac{r_{\mathrm{D}}^{e}}{r_{\mathrm{D}}}\right) + \beta_{\mathrm{D}}\left(\frac{1}{r_{\mathrm{D}}} - \frac{1}{r_{\mathrm{D}}^{e}}\right)\right)\right]^{1/2}}{Q_{\mathrm{D}}}, \tag{A.13}$$

where

$$r_{\mathrm{D}}^{e} = \frac{r_e}{r_{\mathrm{w}}}. \tag{A.14}$$

If we introduce a constant density in Equation (A.8), we have the simple steady-state solution

$$P_{\mathrm{D}} = \ln\left(\frac{r_{\mathrm{D}}^{e}}{r_{\mathrm{D}}}\right) + \beta_{\mathrm{D}}\left(\frac{1}{r_{\mathrm{D}}} - \frac{1}{r_{\mathrm{D}}^{e}}\right). \tag{A.15}$$

Appendix B. Derivation of Characteristic Distances of non-Darcy Fracture/Matrix Flow with the Double-porosity Model

We assume that at a given time non-Darcy flow of single-phase slightly compressible fluid within rock matrix is subject to quasi-steady state flow condition, that is, decrease or increase rate in pressure with time inside rock matrix reaches a constant. The non-Darcy flow within matrix is then described by combining Equations (2.1) and (2.2), for example, to a 1-D case, as

$$\frac{\partial}{\partial x}\left[-\frac{\mu}{2k\beta}\left\{1 - \left[1 + \frac{4k^2\rho\beta}{\mu^2}\frac{\partial P}{\partial x}\right]^{1/2}\right\}\right] = \phi_{\mathrm{i}} C_{\mathrm{t}} \frac{\partial P}{\partial t}. \tag{B.1}$$

Under quasi-steady state condition, the right-hand side of Equation (B.1) is a constant. The left-hand side of (B.1) may be approximated, for purpose of evaluating a characteristic length, as,

$$\begin{aligned}
&\frac{\partial}{\partial x}\left[-\frac{\mu}{2k\beta}\left\{1 - \left[1 + \frac{4k^2\rho\beta}{\mu^2}\frac{\partial P}{\partial x}\right]^{1/2}\right\}\right] \\
&\quad = \frac{\partial}{\partial x}\left[-\frac{\mu}{2k\beta}\left\{1 - \left[1 + \frac{4k^2\rho\beta}{2\mu^2}\frac{\partial P}{\partial x} + \cdots\right]\right\}\right] \\
&\quad \approx \frac{\partial}{\partial x}\left[-\frac{\mu}{2k\beta}\left\{1 - \left[1 + \frac{2k^2\rho\beta}{\mu^2}\frac{\partial P}{\partial x}\right]\right\}\right] = \frac{k}{\mu}\frac{\partial^2 P}{\partial x^2}.
\end{aligned} \tag{B.2}$$

The critical assumption used in (B.2) is the linearization of the nonlinear term of the non-Darcy flow. The rationale behind the approximation is that matrix permeability is normally several orders of magnitude lower than fracture permeability, the term in the right-hand side of (B.2), describing non-Darcy flow, becomes

$$\frac{2k^2\rho\beta}{\mu^2}\frac{\partial P}{\partial x} \ll 1. \tag{B.3}$$

Then, higher-order terms in the Tailor series in (B.2) may be ignored. This approximation can be further examined using the correlation (5.1) for non-Darcy flow coefficient versus permeability and porosity with common parameter values (in SI unit)

$$\begin{aligned}\frac{2k^2\rho\beta}{\mu^2}\frac{\partial P}{\partial x} &= \frac{2C_\beta\rho k^{3/4}}{\mu^2}\\ &= \frac{2\times(C_\beta=10^{-8})\times(\rho=1000)\times(k=10^{-14})^{3/4}}{(\mu=0.001)^2}\left(\frac{\partial P}{\partial x}\right)\\ &= 6.3\times10^{-10}\left(\frac{\partial P}{\partial x}\right). \end{aligned} \tag{B.4}$$

Therefore, as long as the pressure gradients inside matrix are less that 1,000 bars m^{-1} (or $10^8\,Pa\,m^{-1}$), which is almost always true for any given fracture/matrix systems, Equation (B.3) is a reasonable assumption. With this linearization, flow inside matrix under a quasi-steady-state condition is then described by

$$\frac{\partial^2 P}{\partial x^2} = \text{const}, \tag{B.5}$$

that is, the flow in the matrix is approximated as Darcy flow.

Similarly, it is easy to show that other-type 1-D flow (e.g. radial or spherical) or multi-dimensional flow inside matrix flow becomes linear, Darcy-type flow. Therefore, characteristic lengths derived for numerical calculation of Darcy flow crossing fracture/matrix interfaces with the double-porosity method (Pruess, 1983; Wu and Pruess, 1988) can be directly extended into non-Darcy flow cases, as summarized in Table I. This is because these values of characteristic lengths are simply determined using the same flow equation for a given shape of matrix blocks.

Acknowledgements

The author is indebted to Jianchun Liu and Dan Hawkes for their careful and critical review of this manuscript. Thanks are also due to Prof. J. R. A. Pearson and the other two anonymous reviewers for their critical and instructive comments and suggestions for improving this paper. This work was supported in part by the Assistant Secretary for Energy Efficiency and Renewable Energy, Office of Geothermal and Wind Technologies of the U.S. Department of Energy, under Contract no. DE-AC03-76SF00098.

References

Aziz, K. and Settari, A.: 1979, *Petroleum Reservoir Simulation,* Applied Science, London.

Arbogast, T.: 1993, Gravitational forces in dual-porosity systems: I. model derivation by homogenization, *Transport in Porous Media* **13**(2), 179–203.

Barenblatt, G. I., Zheltov, I. P. and Kochina, I. N.: 1960, Basic concepts in the theory of seepage of homogeneous liquids in fissured rocks, PMM, *Sov. Appl. Math. Mech.* **24**(5), 852–864.

Douglas, Jr., J., Arbogast, T., Paes-leme, P. J., Hensley, J. L. and Nunes, N. P.: 1993, Immiscible displacement in vertically fractured reservoirs, *Transport in Porous Media* **12**(1), 73–106.

Douglas, Jr., J., and Arbogast, T.: 1989, Two models for the waterflooding of naturally fractured reservoirs, in: *SPE 18425, Presented at the 1989 10 SPE Symposium on Reservoir Simulation*, 6–8 February, Houston, Texas.

Earlougher, Jr., R. C.: 1977, *Advances in Well Test Analysis*, SPE Monograph, SPE of AIME, Dallas, Vol. 5.

Evans, E. V. and Evans, R. D.: 1988, Influence of an immobile or mobile saturation on non-Darcy compressible flow of real gases in propped fractures, *J. Petrol. Technol.* **40**(10), 1343–1351.

Evans, R. D., Hudson, C. S. and Greenlee, J. E.: 1987, The effect of an immobile liquid saturation on the non-Darcy flow coefficient in porous media, *J. SPE Prod. Engng Trans. AIME* **283**, 331–338.

Forsyth, P. A., Wu, Y. S. and Pruess, K.: 1995, Robust numerical methods for saturated-unsaturated flow with dry initial conditions in heterogeneous media, *Adv. Water Resour.* **18**, 25–38.

Guppy, K. H., Cinco-Ley, H., Ramey, Jr., H. J. and Samaniego, F.: 1982, Non-Darcy flow in wells with finite-conductivity vertical fractures, *Soc. Pet. Eng. J.* 681–698.

Guppy, K. H., Cinco-Ley, H. and Ramey, Jr., H. J.: 1981, Effects of non-Darcy flow on the constant-pressure production of fractured wells, *Soc. Pet. Eng. J.* 390–400.

Katz, D. L. and Lee, R. L.: 1990, *Natural Gas Engineering, Production and Storage*, Chemical Engineering Series, McGraw-Hill, New York.

Kazemi, H.: 1969, Pressure transient analysis of naturally fractured reservoirs with uniform fracture distribution, *SPEJ* 451–462; *Trans. AIME* 246.

Lai, C. H., Bodvarsson, G. S., Tsang, C. F. and Witherspoon, P. A.: 1983, A new model for well test data analysis for naturally fractured reservoirs, in: *SPE 11688, Presented at the 1983 California Regional Meeting*, 23–25, March, Ventura, California.

Lee, R. L., Logan, R. W. and Tek, M. R.: 1987, Effetcs of turbulence on transient flow of real gas through porous media, *SPE Format. Eval.* 108–120.

Liu, X., Civan, F. and Evans, R. D.: 1995, Correlations of the non-Darcy flow coefficient, *J. Canad. Petrol. Technol.* **34**(10), 50–54.

Muskat, M.: 1946, *The Flow of Homogeneous Fluids through Porous Media*, J. W. Edwards, Ann Arbor, Michigan.

Pruess, K.: 1991, TOUGH2 – A general-purpose numerical simulator for multiphase fluid and heat flow, Report LBL-29400, Lawrence Berkeley National Laboratory, Berkeley, California.

Pruess, K. and Narasimhan, T. N.: 1985, A practical method for modeling fluid and heat flow in fractured porous media, *Soc. Pet. Eng. J.* **25**, 14–26.

Pruess, K.: 1983, GMINC – A mesh generator for flow simulations in fractured reservoirs, Report LBL-15227, Lawrence Berkeley National Laboratory, Berkeley, California.

Scheidegger, A. E.: 1972, *The Physics of Flow through Porous Media*, University of Toronto Press.

Skjetne, E., Statoil, T. K. and Gudmundsson, J. S.: 1999, Experiments and modeling of high-velocity pressure loss in sandstone fractures, In: *SPE 56414, Presented at the 1999 SPE Annual Technical Conference and Exhibition*, 3–6, October, Houston, Texas.

Swift, G. W. and Kiel, O. G.: 1962, The prediction of gas-well performance including the effects of non-Darcy flow, *J. Petrol. Technol. Trans. AIME* **222**, 791–798.

Tek, M. R., Coats, K. H. and Katz, D. L.: 1962, The effects of turbulence on flow of natural gas through porous reservoirs, *J. Petrol. Technol. Trans. AIME* **222**, 799–806.

Wang, X. and Mohanty, K. K.: 1999, Multiphase non-Darcy flow in gas-condensate reservoirs, In: *SPE 56486, Presented at the 1999 SPE Annual Technical Conference and Exhibition*, 3–6, October, Houston, Texas.

Warren, J. E., and Root, P. J.: The behavior of naturally fractured reservoirs, *Soc. Pet. Eng. J. Trans. AIME* **228**, 245–255.

Wu, Y. S.: 2000a, A virtual node method for handling wellbore boundary conditions in modeling multiphase flow in porous and fractured media, LBNL-42882, *Water Resour. Res.* **36**(3), 807–814.

Wu, Y. S.: 2000b, *Non-Darcy Displacement of Immiscible Fluids in Porous Media*, LBNL-45228, Lawrence Berkeley National Laboratory, Berkeley, California.

Wu, Y. S., MSFLOW: 1998, *Multiphase Subsurface Flow Model of Oil, Gas and Water in Porous and Fractured Media with Water Shut-off Capability*, *Documentation and User's Guide*, Walnut Creek, California.

Wu, Y. S. and Pruess, K.: 1998, A multiple-porosity method for simulation of naturally fractured petroleum reservoirs, *SPE Reserv. Engng* **3**, 327–336.